RSC Advances

PAPER

View Article Online
View Journal | View Issue

Cite this: *RSC Adv.*, 2026, **16**, 4347

Systematic evaluation of a novel mesoporous silica nanoparticles (MSNs)-*Spirulina platensis* nanohybrid for breast cancer treatment: mechanistic investigation *via* pharmacological network analysis

Dina S. Ghallab, *[a] Doaa A. Ghareeb,[bcd] Mazen Sherif [b] and Marwa Y. Kenawy[e]

Breast cancer continues to be one of the world's most deadly diseases among women, with a high incidence rate. Thus, searching for safe and effective treatment is urgently needed. *Spirulina platensis*, which is packed with an astonishing variety of bioactive compounds, may present a decent option against this crippling disorder. Accordingly, the current work innovatively integrated network pharmacology and nanoscience to pinpoint multi-target pharmacological effects of *Spirulina* bioactives and enhance their stability and anticancer effectiveness *via* a mesoporous silica nanoparticles (MSNs) framework. Network pharmacology analysis illuminated AKT1, SRC, IGFR 1, BCL-2, and EGFR as the core target genes that are typically enriched in microRNAs in cancer, PI3K-Akt signaling, and EGFR tyrosine kinase inhibitor resistance pathways, and they are associated with the multi-wave mechanism of *Spirulina* compounds against breast cancer. Complementarily, a nanohybrid platform of MSNs and *Spirulina* extract (SP@MSNs) was established and assessed using different structural and morphological analyses, primarily SEM, TEM, EDX, XRD, FTIR spectroscopy, BET, zeta size and potential analyses and TGA, followed by screening against normal and breast cancerous cells using the MTT assay. This biocompatible nanocomposite revealed optimal physicochemical properties regarding size, shape, surface charge, and chemistry, and it exhibited promising loading capacity (LC%) and encapsulation efficiency (EE%) scores of 78.07% and 98.37%, respectively. SP@MSNs showed a 3.5-fold increase in anti-breast cancer action ($IC_{50} = 33.6 \pm 0.32$ μg mL^{-1}) compared to *Spirulina* extract alone. MSNs enhanced the *Spirulina* compounds' stability, solubility, and cellular uptake, maximizing anticancer efficacy. These findings reveal the significance of the synergy between nanotechnology and network pharmacology to establish a multifaceted drug discovery framework and a high-precision delivery system for breast cancer therapy. Nevertheless, continued interdisciplinary research is crucial for bolstering its biological relevance.

Received 17th November 2025
Accepted 1st January 2026

DOI: 10.1039/d5ra08876c

rsc.li/rsc-advances

1. Introduction

In the view of the 2023 global cancer annual report, breast cancer continues to be one of the world's most preventable and deadly diseases among women, and its incidence rate continues to rise annually, even with the advancements in therapy.[1] Despite revolutionary efforts manifested by surgical resection, targeted chemotherapy, and immunotherapy to minimize such oncological disorders, the high recurrence rate and emergence of drug resistance during some phases of tumorigenesis, coupled with the lack of distinction of some conventional chemotherapeutics among neoplastic and normal cells[2] and thus their limited success rate, have driven the scientific community to extensively explore new non-toxic, selective, and more effective alternative approaches to combat this severe pathology that poses a real threat to human health.

Undoubtedly, the marine ecosystem can present many options that may be used to fight this crippling disorder.[3] Marine microalgae, primarily blue-green algae (Cyanobacteria), which are abundant in coastal regions, serve as a vast

[a]*Department of Pharmacognosy, Faculty of Pharmacy, Alexandria University, Alexandria 21521, Egypt. E-mail: Dinaghallab6@gmail.com; Dina.Ghalab@alexu.edu.eg; Tel: +0201080919812*

[b]*Bio-screening and Preclinical Trial Lab, Biochemistry Department, Faculty of Science, Alexandria University, Alexandria, Egypt*

[c]*Center of Excellence for Drug Preclinical Studies (CE-DPS), Pharmaceutical and Fermentation Industry Development Center, City of Scientific Research and Technological Applications (SRTA-City), New Burg El-Arab City, Alexandria, Egypt*

[d]*Research Projects Unit, Pharos University, Alexandria 21934, Egypt*

[e]*Fabrication Technology Research Department, Advanced Technology and New Materials Research Institute (ATNMRI), City of Scientific Research and Technological Applications (SRTA-City), New Borg El-Arab, Alexandria 21934, Egypt*

community of photosynthetic organisms with a wide variety of morphologies and functions.[4] Beyond their importance as primary producers of most aquatic food chains in the blue planet and their essential role in biogeochemical cycling, microalgae metabolites, including polysaccharides, terpenoids, carotenoids, phytosterols, and phenolics, have attracted unprecedented levels of interest from medicinal chemistry experts because of their structural distinctiveness and range of functions.[5] Among the microalgae with matrices that are high in bioactive chemicals, *Spirulina platensis* is used as a supplemental medicine and traditional food in many Asian nations because of its various health benefits and rich nutritional makeup.[6] In addition to its frequent dietary consumption, *Spirulina* is one of the most important components of marine phytoplankton, packed with unexplored and environmentally sustainable bioactive compounds with a wide range of biofunctionalities, such as anticancer, anti-inflammatory, antioxidant, antidiabetic, antimicrobial, anticoagulant, and neuroprotective properties.[7–9] Paralleling previous investigations concerning the cytotoxic potential of *Spirulina*, the hydroethanolic extract of *S. platensis* displayed cytotoxic potential in colon carcinoma cells (HCT116) and hepatocellular carcinoma cells (HEPG2) with IC_{50} of 18.8 and 22.3 μg mL^{-1} by inducing apoptosis and severe mitochondrial damage.[10] Further, the water extract of *Spirulina* has been highlighted for its extraordinary cytotoxicity against the human non-small-cell lung carcinoma A549 cell line by directly acting on the cell cycle/apoptosis pathway, reducing phosphorylation of Akt and Rb proteins and the expression of cyclin D1 and CDK4, as well as increasing the Bax to Bcl-2 ratio in the A549 cells.[11] All these investigations strongly support the conclusion that *S. platensis* serves as a prodigiously rich source of high-value compounds with outstanding anti-cancer activity. However, the diversified molecular mechanisms beyond the efficacy of *S. platensis* against breast cancer remain elusive. Hence, further research is warranted to develop the full potential of marine natural products for breast cancer mitigation.

In this regard, network pharmacology has evolved as a comprehensive biological discipline coupling multi-scale pharmacology with system biology to explore drug action mechanisms from a molecular aspect.[12] The combined application of network pharmacology and metabolomics closely follows the holistic perspective of traditional Chinese medicine, wherein multi-target synergy treatment can comprehensively profile the biological connections among compounds, genes, metabolites and metabolic pathways, thereby facilitating the identification of the overall action mechanisms and revealing novel therapeutic targets in a deeper scientific language.[12] An overview of earlier investigations reveals a paucity of network pharmacology analyses on*Spirulina* chemical entities for ameliorating and combating breast cancer.

Although *Spirulina* serves as a prime repository of bioactive compounds with potential significance and immense prospects for drug development against breast cancer, the current development of therapeutic agents from marine flora continues to face bottlenecks.[13] Apart from obtaining a sustainable and sufficient supply of marine compounds, the poor water solubility of these compounds limits their pharmaceutical applications in cancer therapy.[13] To address these issues in biomedical programs, nanotechnology can offer an insightful approach with distinct benefits over the systemic administration of free natural bioactive molecules. These benefits primarily involve improving the water solubility of the hydrophobic natural marine medications, enhancing their permeability, release profiles, and retention effects, as well as improving the tumor-targeting efficiency, biological potential, and safety profile of the agents.[14] Further, encapsulation of hydrophobic drugs into nanoparticles (<200 nm) can significantly improve drug dispersion in water and delivery to specific tumorous sites.[15] More specifically, mesoporous silica nanoparticles (MSNs), composed of silicon dioxide, have various applications in biomedicine for drug delivery, biosensing, and imaging, as well as in agriculture and as industrial additives.[16] They possess tunable properties such as ease of surface modification, good mechanical stability, and high-capacity loading.[17] Essentially, the encapsulation of a natural extract into mesoporous silica nanoparticles (MSNs) creates a biocompatible nano-system that enhances the effectiveness of the natural compounds by improving their stability, bioavailability, and targeted delivery, especially for anticancer therapies.[17] A review of previous reports reveals that numerous marine-derived constituents have been encapsulated in MSNs, and they exert remarkable anticancer potential.[16] For instance, a recent study has proven that diatom-based mesoporous silica nanoparticles (MSNs) improve targeted drug delivery, enhance therapeutic efficacy, and offer a more biocompatible and eco-friendly alternative to synthetic materials in cancer therapy.[18] Another study has demonstrated that marine polysaccharides, primarily fucoidans, encapsulated in MSNs have superior anticancer effects against colon cancer cells compared to free fucoidans.[19] However, incorporating *Spirulina* extract within the porous structure of silica nanoparticles to enhance its stability, solubility, and cellular uptake across cancer cells remains overlooked and demands further investigation.

To fill these gaps, the current work offers a synergistic strategy featuring network pharmacology and nanotechnology, followed by experimental verification to systematically uncover the multi-target mechanisms of *Spirulina* on breast cancer at the molecular level and rationally assess the anti-tumor potential of MSN-*Spirulina* nanoconjugates against breast cancer *in vitro.* For clarity, network pharmacology analysis was first conducted to systematically reveal the multi-target mechanisms of *Spirulina* bioactive constituents against breast cancer by creating the "Components-genes-pathway" network. Next, *Spirulina* extract was loaded into silica nanoparticles, creating an optimized nano-conjugate for breast cancer. An *in vitro* cytotoxic screening of *Spirulina* extract and its nano-formulation on breast cancer cell lines was then performed using a 3-(4,5-dimethylthiazol-2-yl)-2,5-diphenyltetrazolium bromide (MTT) assay to validate the network findings and assess the therapeutic effectiveness of the established nano-system in breast cancer mitigation.

This study will provide vital stepping stones for broader mechanism investigations of the efficacy of *Spirulina*

constituents. These bioactivities can be used as reference templates for the green synthesis of nanoparticles and the commercialization of stable, efficient, and affordable anti-cancer agents as suitable substitutes for costly breast cancer treatments.

2. Materials and methods

2.1. Chemicals and reagents

N-Cetyl-*N*,*N*,*N*-trimethyl ammonium bromide (CTAB: purity 98%) obtained from Alpha Chemika (India) as a cationic surfactant. The precursor solution tetraethyl orthosilicate (TEOS) was obtained from Merck (Germany). Ethyl alcohol (absolute; assay ≥99.8%) was purchased from Sigma-Aldrich (USA). Ammonia solution (concentration 35%) was from Fisher Scientific (USA), and sodium hydroxide (assay 97%) was purchased from Fluka (Switzerland). Phosphate-buffered saline (PBS), Dulbecco's modified Eagle medium (DMEM), 3-(4,5-dimethylthiazol-2-yl)-2,5-diphenyltetrazolium bromide (MTT), heat-deactivated fetal bovine serum (FBS), antibiotics (penicillin 100 U/mL, streptomycin 10 μg mL^{-1}) and sodium pyruvate (1 mM) were from Sigma-Aldrich (St. Louis, Mo, USA). Human Foreskin Fibroblasts (HSF) and breast cancer cell line (MCF-7) were purchased from the National Cancer Institute (NCI), Cairo, Egypt. Analytical-grade chemicals and solvents were also utilized.

2.2. Network pharmacology analysis

2.2.1. Compilation of *S. platensis* constituents and filtration based on ADME and drug-likeness indices. As an extension of our earlier report implementing UPLC-MS-based chemical analysis of *S. platensis* and concluding with a thorough metabolites annotation of 65 compounds belonging to different classes, mostly fatty acids and their derivatives, amino acids, terpenoids, along with significant amounts of polyphenolics,[20] these diverse characterized compounds were designated as candidate compounds for the network pharmacology analysis. Firstly, the compounds were submitted into Qikprop software (Schrödinger suite 2017A) for virtual filtration based on their oral bioavailability (OB) and Lipinski's rule of five parameters; compounds that met more than three of Lipinski's rule of five criteria and had a favourable OB score of at least 30% were chosen as potential candidates for further investigation.

2.2.2. Potential targets, gene prediction and PPI network construction. STITCH DB (http://stitch.embl.de/, ver. 5.0) and SwissTargetPrediction (possibility >0.4) were utilized for potential target gene prediction of the selected compounds with the species specified as "*Homo sapiens*". Coincidently, the gene profile tightly implicated to breast cancer was retrieved from GeneCards (https://www.genecards.org/) and therapeutic target database (TTD) (http://db. idrblab.net/ttd/) using the term "breast cancer" where the intersection targets obtained from the Venn platform was imported into STRING (https://string-m.org, updated on January 19, 2019) database specifying human species and a confidence level of 0.7 for protein–protein interactions (PPIs) network building.

2.2.3. KEGG pathway enrichment analysis. The core genes chosen above were directly uploaded onto the Database for Annotation, Visualization and Integrated Discovery (DAVID) 2021 (https://david.ncifcrf.gov/home.jsp) database for Kyoto Encyclopedia of Genes and Genomes (KEGG) pathway enrichment analysis, to clarify the biological functions and possible mechanisms of the pinpointed potential genes.

Eventually, with a scope to fully decipher the pharmacological mechanisms of *S. platensis* compounds against breast cancer, the pharmacological networks identified above were created and examined visually using Cytoscape software (version 3.7.2, http://www.cytoscape.org/, Boston, MA, USA), wherein the Network Analyzer plug-in was used to monitor the degree centrality (DC), network centrality (NC), and local average connectivity (LAC). Notably, the nodes' significance in each constructed network was indicated by high scores in these parameters.

2.3. Sample collection and preparation

In a follow-up series of experiments, *S. platensis* that was gathered in the summer of 2022 from the coastal region of Abu-Qir, Alexandria, North Egypt, and taxonomically recognized in our earlier LC-MS investigation,[20] was chosen for cytotoxic screening on the breast cancer cell line (MCF-7). First, the freeze-dried *Spirulina* specimens were finely ground, sieved through a 50-mesh, precisely weighed, and subjected to an extraction process following our previously reported protocol[20] with minor modifications. In short, 100 g of *Spirulina* powder was suspended in 350 mL of 70% ethanol and ultrasonicated at 40 °C for 90 min, and the process was repeated twice. After mixing, the extracts were filtered and vacuum-concentrated at 40 °–50 °C until dry.

2.4. Biosynthesis and characterisation of *S. platensis* loaded within MSNs (SP@MSNs)

2.4.1. Preparation of MSNs. Biodegradable MSNs were synthesized through a modified sol–gel method using cetyltrimethylammonium ammonium bromide (CTAB) as a template under alkaline conditions with tetraethoxysilane (TEOS) as a co-silica source. The following procedure was used to synthesize the MSNs powder: Initially, 1.15 g CTAB was dissolved in an alkaline aqueous solution (45 mL distilled water, 20 mL absolute ethanol, and 10 mL 35% ammonium solution) and stirred at 300 rpm for 15 min to allow the formation of cationic micelles, which acted as structure-directing agents:

$$\mathrm{CTAB}_{(aq)} \xrightarrow[15\ \mathrm{min}]{\text{alkaline medium}} \text{CTAB micelles} \quad (1)$$

Subsequently, 1 mL of TEOS solution was added dropwise to the reaction mixture under continuous stirring. In the alkaline medium, TEOS undergoes base-catalyzed hydrolysis to form silanol species:

$$\mathrm{Si(OC_2H_5)_4 + 4H_2O \xrightarrow{OH^-} Si(OH)_4 + 4C_2H_5OH} \quad (2)$$

The generated silanol groups condense during stirring at 300 rpm for 2 h, resulting in the formation of a siloxane network around the CTAB micellar template:

$$\equiv Si - OH + HO - Si \equiv \rightarrow \equiv Si - O - Si \equiv + H_2O \quad (3)$$

The cooperative self-assembly between silica species and CTAB micelles leads to the formation of an ordered mesostructured composite (white precipitate):

$$CTAB\ micelles + Si(OH)_4 \rightarrow CTAB@SiO_2 \quad (4)$$

Finally, the white precipitate products were collected, washed three times with distilled water at 6000 rpm for 20 min, and dried. Removal of the CTAB template by calcination in a muffle furnace at 550 °C for 3 h yielded ordered mesoporous silica nanoparticles (MSNs):

$$CTAB@SiO_2 \rightarrow Mesoporous\ SiO_2\ (MSNs) \quad (5)$$

2.4.2. Preparation of S. platensis extract-loaded MSNs (SP@MSNs). *Spirulina* ethanolic extract was loaded onto MSNs through adsorption driven by surface interactions between *Spirulina* biomolecules (SP) and the silanol groups of the mesoporous silica (MSNs). Spirulina contains proteins, polysaccharides, phenolics, and pigments, bearing hydroxyl, amino, and carboxyl functional groups. The loading steps were: 30 mg of MSNs were dispersed in 10 mL of distilled water at 300 rpm for 2 h. At the same time, 10 mL of an absolute ethanol solution containing extract (SP) (5 mg mL^{-1}) was stirred at 300 rpm for 2 h, then added dropwise to the MSNs solution, and the mixture was stirred gently at 300 rpm at room temperature for 24 h. Hydrogen bonding between the surface silanol groups and the hydroxyl-containing *Spirulina* components represents the dominant interaction mechanism:

$$\equiv Si - OH + HO - R_{(Spirulina)} \rightleftharpoons \equiv Si - OH\cdots HO - R \quad (6)$$

This interaction results in the adsorption of *Spirulina* biomolecules on the external surface and within the mesoporous channels of MSNs, forming *Spirulina*-loaded mesoporous silica (SP@MSNs):

$$MSNs + Spirulina\ extract \rightarrow SP@MSNs \quad (7)$$

The SP@MSNs precipitate was obtained through centrifugation at 6000 rpm for 20 min. The amount of extract in the supernatant was measured using a UV-Visible spectrophotometer (UV-2401 PC, Shimadzu, Tokyo, Japan). A calibration curve was prepared using known concentrations of the SP extract (2.5, 5, 10, 15, 20 mg), and the absorbance of the marker compound (*e.g.*, phycocyanin at 620 nm) was measured, as shown in Fig. S1.[21] The loading capacity (LC) and encapsulation efficiency (EE) were calculated according to the following formulas:[22]

$$Amount\ loaded\ (mg) = total\ extract\ added\ (mg) - amount\ remaining\ in\ supernatant \quad (8)$$

$$Loading\ capacity(LC, wt\%) = \frac{amount\ \ loaded\ (mg)}{mass\ of\ loaded\ MSNs\ (mg)} \times 100\% \quad (9)$$

$$Encapsulation\ efficiency(EE,\%) = \frac{amount\ loaded\ (mg)}{total\ extract\ added\ (mg)} \times 100\% \quad (10)$$

2.4.3. The scanning electron microscopy (SEM). Gold sputter-coating was applied to the SP, MSNs, and SP@MSNs prior to microscopic investigation using scanning electron microscopy (SEM, JEOL JSM 6360LA, Japan).[23]

2.4.4. Transmission electron microscopy (TEM) and energy-dispersive X-ray analysis (EDX). The morphology and the elemental analysis of the SP, MSNs, and SP@MSNs were analyzed using a transmission electron microscope (JEOL 2100 PLUS, Japan) at an accelerating voltage of 300 kV. Energy-dispersive X-ray analysis (EDX, Gatan, Pleasanton, CA, USA) was also performed. Transmission electron microscopy (TEM) samples were prepared by dropping a diluted solution of absolute ethanol containing SP, MSNs, and SP@MSNs separately on a TEM grid, followed by air drying. TEM images were obtained without staining.[24]

2.4.5. X-ray diffraction analysis (XRD). The SP@MSNs, free MSNs and free SP extract were subjected to XRD analysis. The X-ray diffractograms were acquired using an XRD diffractometer (XRD-6100 Shimadzu, Japan),[23] with CuKα radiation, a voltage of 30 kV, and an electric current of 30 mA. The scans were performed at 2°/min for 2θ values 10° to 80°.

2.4.6. Fourier-transform infrared (FTIR) spectroscopic analysis. FTIR spectra of SP, MSNs, and the SP@MSNs complex were recorded with a Shimadzu IRTracer-100 spectrophotometer (FTIR, Shimadzu, Japan) using the KBr pellet method, within the wavenumber range of 400–4000 cm^{-1}.

2.4.7. Thermal stability profile using thermo-gravimetric analysis (TGA). A thermo-gravimetric analyser (TGA-50 Shimadzu, Tokyo, Japan) was used to examine the thermal behaviour of the free SP extract, MSNs, and SP@MSNs samples. Each sample was carefully weighed (4 mg) using a microbalance, and the temperature program was run from 0 °C to 800 °C at a heating rate of 10 °C min^{-1}.

2.4.8. Determination of particle size using dynamic light scattering (DLS). The SP, MSNs, and (SP@MSNs) synthesized formulations' hydrodynamic diameter and size distribution were determined using a Zetasizer (Nano ZS, Malvern Instruments, UK).[21,25] The samples were analysed at 25 °C with a detection angle of 90°, and the viscosity and refractive index values used were those of absolute ethanol. A polydispersity index (PDI) was also obtained as part of this approach, which provides information on the sample's polydispersity.

2.4.9. Determination of the zeta potential. The surface charge of the SP, MSNs, and SP@MSNs samples was determined at ambient temperature using a Zetasizer Nano ZS

(Malvern Instruments, Malvern, UK). The zeta potential values were calculated based on the electrophoretic mobility of the nanoparticles under an applied electric field. The refractive indices used for the measurements were 1.36 and 1.50.[21]

2.4.10. Determination of the pore size and surface area. The pore volume, pore diameter, and specific surface area of empty mesoporous silica nanoparticles (MSNs) and SP-loaded MSNs (SP@MSNs) were determined by nitrogen adsorption–desorption analysis using a quick automated surface area and pore size analyzer (BELSORP MINI X, Microtrac MRB, Japan). The specific surface area was calculated using the Brunauer–Emmett–Teller (BET) method, while the pore size distribution and pore volume were evaluated using the Barrett–Joyner–Halenda (BJH) model.

2.5. MTT cytotoxicity assay

Human Foreskin Fibroblasts (HSF) and breast cancer cell lines (MCF-7) obtained from the National Cancer Institute (NCI) were routinely maintained in DMEM media fortified with 10% (v/v) heat-deactivated FBS, penicillin 100 U per mL and streptomycin 10 μg mL^{-1}, as well as 1 mM sodium pyruvate, in a 5% CO_2-humidified air atmosphere incubator at 37 °C.

The cytotoxicity towards normal cells is a critical issue in anti-cancer investigations to determine the selective toxicity of the screened drug to cancer cells.[26] For our investigation, *Spirulina* extract, silica nanoparticles, and the encapsulated nano-formula were tested on normal cell lines (HSF) to determine their specific cytotoxicity and safety profiles, leading to more targeted therapies. Subsequently, *Spirulina* extract and its encapsulated MSNs nano-formula were screened against cancerous breast cancer cells (MCF-7) to explore the anticancer potential of *Spirulina* extract, both in its crude form and incorporated into MSNs nano-formulation.

The MTT assay was conducted by following a previous protocol with minor adjustments.[27] For the test, normal and cancerous cells were separately seeded in a 96-well microtiter plate at an approximate density of 2×10^5 cells/well. Master stock solutions of the tested samples (10 mg mL^{-1}) were prepared, then diluted with culture medium into the working concentrations (500, 250, 125, 62.5, 31.25 and 15.6 μg mL^{-1}). 50 μL of each prepared concentration was supplied to both normal and tumor cells in triplicate. In other domains, negative controls spiked with 50 mL culture medium and DMSO (0.5%) were prepared without any tested treatments. After that, the cells were incubated for 72 hours, and 10 μL of MTT reagent (5 mg mL^{-1} in PBS) was then added to each well, followed by a 4-hours incubation. Lastly, the medium was discarded, and DMSO (100 μL) was added to dissolve formazan crystals in each well. Cell viability was estimated by measuring absorbance at 495 nm using a Benchmark microplate reader (Molecular Devices Corporation, USA). The median growth inhibitory concentration (IC_{50}) for each tested sample was measured using the software Prism 8.0 (GraphPad Software).

2.6. Statistical analysis

Every experiment was conducted in triplicate, and the mean values ± standard deviations (SD) were used to express the results. To determine the statistical difference between the tested samples, a one-way ANOVA was used, followed by Turkey's test; a *P* value of less than 0.05 was deemed statistically significant.

3. Results and discussion

3.1. Fishing out breast cancer-associated genes of *spirulina* constituents

Network pharmacology is emerging as a frontier paradigm integrating computational and pharmacological investigations to provide full data regarding pharmacological mechanisms of drugs with multiple components, ultimately guiding drug discovery and development.[28,29]

In the present work, a set of 65 compounds recouped from our previous report regarding *Spirulina* chemical profile through UPLC-QqQ-MS/MS analysis, was preliminarily evaluated by ADME parameters, namely OB and Lipinski's Rule (LR), to pinpoint bioactive molecules with favorable pharmacokinetic attributes. Accordingly, as depicted in Table S1, 39 compounds fulfilling the screening criteria (OB ≥ 30% and satisfying at least three of Lipinski's rule (LR) parameters) were selected as candidate constituents for network pharmacology analysis. By searching online genomic databases, mainly STITCH 5.0 and Swiss Target Prediction databases with species assigned as "*Homo sapiens*", 155 interacting targets associated with *Spirulina* constituents were selected. Simultaneously, a search employing the key term "breast carcinoma" in the GeneCards and TTD databases led to the discovery of 3212 disease targets. After integration using a Venn mapping tool, 59 target genes were principally considered as the core targets tightly linked with *Spirulina* constituents and breast cancer management (Fig. 1A). For transparency, Cytoscape 3.7.2 was utilized to analyze the predictive component-target interactions with a combined score cutoff higher than 0.7, visualizing the intricate interactions of these components and their respective therapeutic targets in the simple component-target network, as shown in Fig. 1B. Analysis of the component-target network dissected a total of 75 nodes and 719 edges, of which 16 represent component nodes while the other 59 reflect target nodes, with an average of 4.195 for the number of target genes acting on each component manifesting multiple drug-target interactions. The analysis provides a new step for rational drug discovery for multifactorial diseases such as breast cancer. Table 1 presents the topological parameters of the putative targets. Of note, the full gene names with the species of "*Homo sapiens*" retrieved from the UniProt database and the relevant *Spirulina* constituents are listed in Table S2. Analysis of this complicated network revealed AKT1, SRC, IGFR 1, BCL-2, EGFR, JAK2, TLR2 and KDR as potential targets closely related to the molecular mechanism of *Spirulina* against breast cancer. Meanwhile, catechin, rosmarinic acid, apigenin, quercetin dimethyl ether, carnosic acid, eicosapentaenoic acid and linolenic acid are respective key components with a great degree of centrality that act synergistically to mitigate breast cancer. Contingently, flavonoids such as catechin, apigenin and quercetin have been acknowledged to exert a vast range of

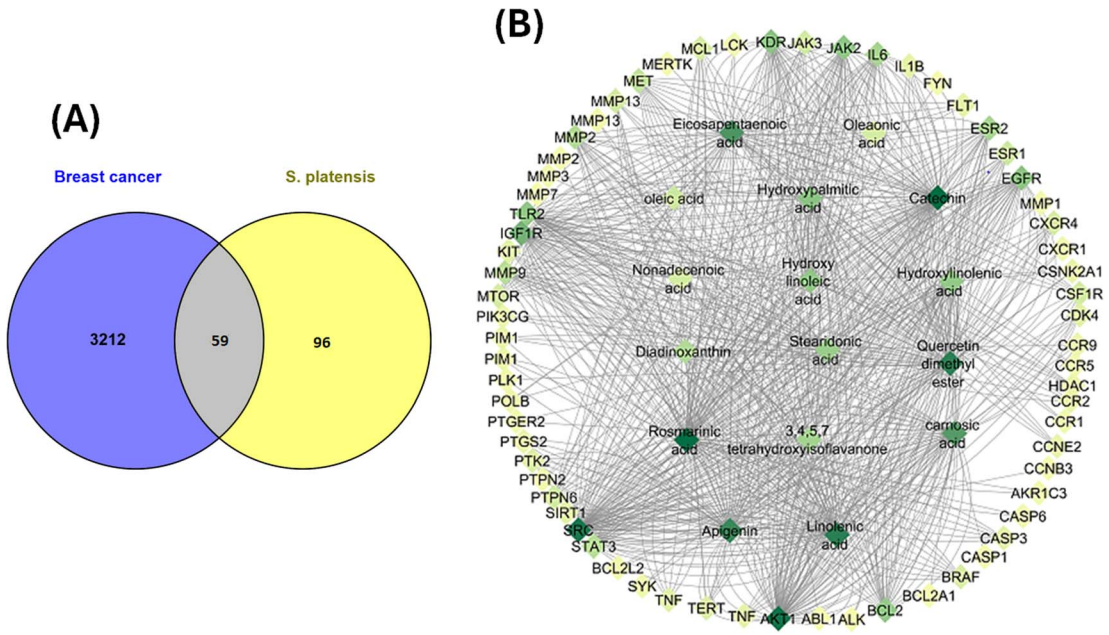

Fig. 1 (A) Venn diagram demonstrating the number of common genes shared between *S. platensis*-related genes and breast cancer genes. (B) *S. platensis*-compounds-target genes interaction network in which the degree value of the nodes is depicted on a color-coded scale from deep to light green.

antioxidant and immune-modulatory actions, potentially exhibiting beneficial effects against breast cancer.[30] The anti-proliferative effects of these promising flavonoids are mainly linked to the induction of cell cycle arrest and apoptosis, typically mediated by the transforming growth factor-β (TGF-β)/Smad pathway.[31] Such effects make these flavonoids ideal candidates for combination cancer therapy with the potential to afford additive anticancer effectiveness and counteract the onset of acquired drug resistance during breast cancer treatment.

In the same context, a recent investigation has demonstrated the putative role of rosmarinic acid in inhibiting breast cell proliferation *via* inducing G1 phase cell cycle arrest and apoptosis, and exacerbating the sensitivity of cell lines resistant to cisplatin, one of the first-line chemotherapeutic agents for breast cancer, suggesting that rosmarinic acid might be an effective multidrug resistance (MDR) reversal agent for breast cancer.[32] Equally important, compelling evidence revealed the noteworthy anticancer activity of polyunsaturated fatty acids (PUFAs), mainly eicosapentaenoic acid (EPA) and linolenic acid (LA), against lung and gastrointestinal carcinomas *via* enhancing DNA damage *via* histone H2AX protein, which is vital in the DNA damage response (DDR) pathway that eventually suppresses cancer progression.[33] Besides this, carnosic acid has been proven to dose-dependently inhibit the proliferation of breast cells through activating apoptosis, autophagy, and Sestrin-2/LKB1/AMPK signalling, along with knocking out the PI3K/AKT/m-TOR signaling pathway in cancerous breast cells.[34,35]

Complementarily, the selected core genes were uploaded onto STRING ver. 10.5, creating a protein–protein interaction (PPI) network, which uncovers functional interactions among multiple targets. The protein–protein interaction network (Fig. 2) encompassing 59 target protein nodes and 792 edges, representing target protein interactions, dissected SRC, IGFR 1, BCL-2, EGFR, AKT1, TLR2 and KDR as the principal genes clustered in the PPI network, affirming their momentous roles in the pathogenesis of breast cancer. Accordingly, targeting these pivotal genes might provide potential therapeutic strategies to combat breast cancer. Principally, emerging evidence has revealed the vital role of SRC in tumor development and metastasis through its regulating role in the cytoskeleton, cell migration, adhesion and invasion in numerous tumor types.[36] Thus, SRC inhibitors might be a promising therapeutic line for breast cancer. Similarly, multiple epidemiological studies have revealed a positive link between circulating IGF-1 levels and various cancer types, such as breast, lung and colon cancer.[37] Mechanistically, it promotes tumor development by suppressing apoptosis and triggering cell proliferation.[37] Equally important, EGFR has been well-acknowledged as exhibiting a fundamentally vital role in epithelial tissue development and homeostasis in the physiological settings.[38] When aberrantly activated in the pathological state, mostly in breast cancer, it aggressively promotes amplification and secondary point mutations at the genomic locus.[38] This evidence opens future therapeutic applications through direct action on the EGFR pathway, which is a prominent molecular target in breast cancer. Undoubtedly, BCL-2 restrains apoptosis, and its inappropriate expression and phosphorylation significantly contribute to cell proliferation, tumor formation and multidrug resistance.[39] Related to this, AKT1 exhibits principal multifaceted roles in different aspects of cellular processes, mainly cell proliferation, survival, migration and metabolism.[40] Further, Akt isoforms play specific roles in cancer cell signaling,

Table 1 The topological parameters of target genes associated with *S. platensis* extract compounds

Gene name	Betweenness centrality	Closeness centrality	Degree	Neighborhood connectivity	Topological coefficient
AKT1	0.046461	0.392523	83	12.71429	0.254658
SRC	0.130598	0.477273	81	13.88889	0.204586
IGF1R	0.032069	0.365217	47	13.8	0.32
KDR	0.035825	0.378378	36	15.6	0.331818
EGFR	0.013118	0.362069	35	19.66667	0.455285
JAK2	0.048301	0.378378	34	13.2	0.277273
TLR2	0.053691	0.381818	33	9.444444	0.205962
BCL2	0.006344	0.308824	32	8.25	0.3625
ESR2	0.153191	0.482759	24	11.07692	0.167949
IL6	0.007447	0.33871	24	15	0.424242
MMP2	0.022088	0.362069	20	11	0.263158
STAT3	4.10×10^{-4}	0.295775	18	13	0.75
MMP9	0.015227	0.344262	18	15	0.4
MET	4.10×10^{-4}	0.295775	15	13	0.75
ESR1	0.059686	0.42	12	14.25	0.254808
MMP13	0.036782	0.407767	10	15.16667	0.277778
PTPN6	0.003381	0.304348	10	7.75	0.375
JAK3	0.00531	0.315789	10	13.5	0.5
CSF1R	0.007284	0.311111	10	13.5	0.543478
CXCR4	0.00513	0.330709	9	14.66667	0.455556
MCL1	0.007097	0.330709	9	13.33333	0.411111
MTOR	0	0.276316	9	14	0
BRAF	0	0.302158	8	21	0
TERT	0.012902	0.330709	7	8.833333	0.290123
PTK2	0	0.295775	7	18	0
SIRT1	4.10×10^{-4}	0.295775	6	13	0.75
KIT	0.016206	0.344262	6	15.66667	0.419048
CDK4	0	0.285714	6	13	0
TNF	0	0.302158	6	21	0
CASP3	0	0.302158	6	21	0
IL1B	0	0.3	5	20	0
TNF	0	0.285714	5	13	0
CSNK2A1	0.011534	0.35	4	13.75	0.354167
PIM1	0.00175	0.320611	4	19	0.666667
CCR2	7.44×10^{-4}	0.297872	4	11	0.588235
HDAC1	0.001301	0.291667	4	8.5	0.535714
PTGS2	0	0.295775	4	18	0
PIK3CG	0	0.3	3	20	0
PIM1	0	0.302158	3	21	0
CCR9	0.001471	0.295775	3	10.5	0.59375
MMP13	0	0.285714	2	13	0
PTGER2	2.26×10^{-4}	0.287671	2	9	0.666667
SYK	0	0.3	2	20	0
MMP3	0.002431	0.308824	2	13	0.545455
PLK1	0.00175	0.320611	2	19	0.666667
AKR1C3	0	0.302158	2	21	0
MMP1	0	0.302158	2	21	0
LCK	0.003967	0.330709	2	19.5	0.596774
CASP6	0	0.302158	2	21	0
CCR1	0	0.276316	2	14	0
CCR5	0	0.276316	2	14	0
CXCR1	0	0.295775	2	18	0
BCL2L2	0	0.285714	2	13	0
MMP7	0	0.285714	1	13	0
ALK	0	0.3	1	20	0
FYN	0	0.302158	1	21	0
MMP2	0	0.302158	1	21	0
BCL2A1	0	0.285714	1	13	0
CASP1	0	0.285714	1	13	0

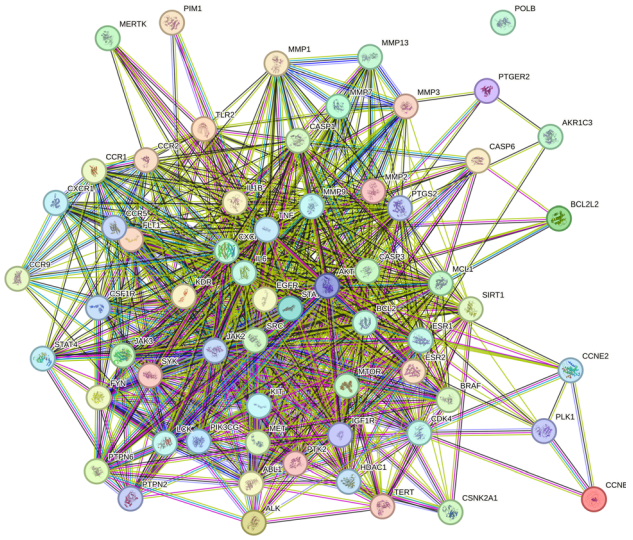

Fig. 2 Protein–protein interaction (PPI) diagram of target genes associated with breast cancer and *Spirulina* extract compounds.

promoting tumor growth and accelerating metastasis.[40] Thereby, opposing the roles of Akt1 as a crucial molecular target in cancer might be an attractive strategy for precision cancer therapy. TLR2 is vital for the detection of hazard signals furnished from cancerous cells' rapidly activating anti-tumor immune response.[41] However, when overactivated, it may lead to an immunosuppressive action that encourages tumor progression.[42] KDR principally mediates the angiogenic switch and metastasis, thereby promoting the survival of cancer cells.[43] Thus, the selective knockout of KDR can prominently manage multiple types of human cancer.

3.2. Prediction of the KEGG signaling pathways of *spirulina* for mitigating breast cancer

Complementarily, KEGG pathway analysis mapping target genes with signaling pathways was conducted to decipher the underlying efficacy mechanisms of *Spirulina* against breast cancer in a concrete scientific language. Given this, a total of 68 KEGG pathways with a significance cutoff of $p < 0.05$ were pinpointed, as clarified in Fig. 3A and Table S3. The top-ranked 20 pathways are depicted in Fig. 3B, revealing that cell proliferation-related pathways, primarily proteoglycan in breast cancer, MicroRNAs in cancer, PI3K-Akt signaling pathway, EGFR tyrosine kinase inhibitor resistance, chemokine signaling pathway, and apoptosis, were intimately implicated. Proteoglycans, the principal molecular effectors of cell surface and pericellular microenvironments, play multiple roles in modulating cancer cell adhesion, migration and neovascularization.[44] The PI3K-Akt signaling pathway is aberrantly activated in cancers and is directly connected with cell proliferation, metastasis and metabolism in tumors.[45] EGFR tyrosine kinase inhibitor resistance, abnormally activated in cancer, plays a crucial role in activating the functions of cancer stem cells (CSCs), including metabolism, immunomodulatory activity, stemness, dormancy, and therapy-resistance.[46] Canonically, EGFR is an oncogene with a significant role in cancer pathogenesis, recurrence, and progression.[38] Chemokines are vital in modulating immune responses and cellular behavior in normal physiology; however, these molecules can promote tumor growth, influence the tumor microenvironment, and negatively impact the efficacy of cancer therapy in the pathological state.[47] Compelling evidence has pointed out that oncogenic changes in breast cancer suppress apoptosis, reducing treatment sensitivity.[47] Thereby, inducing and exploiting apoptosis during multistage

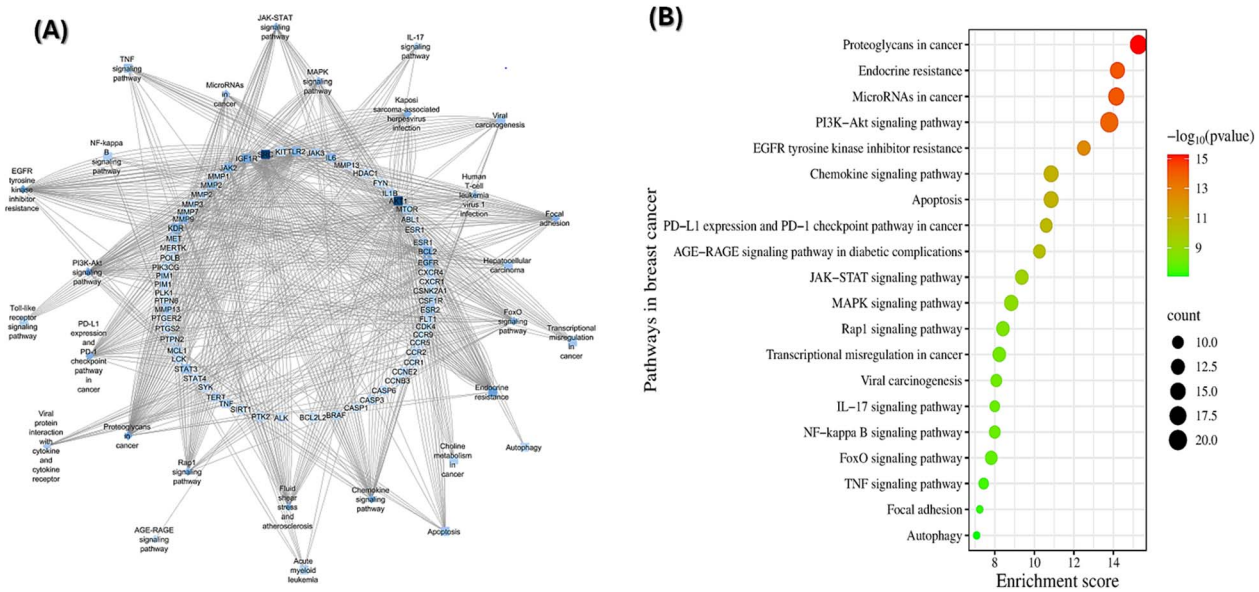

Fig. 3 (A) KEGG pathways - genes network, the color of the node reflects the degree value; the deep color of the nodes reflects the significance degree of the genes and pathways. (B) The top-ranked 20 KEGG pathways based on enrichment score.

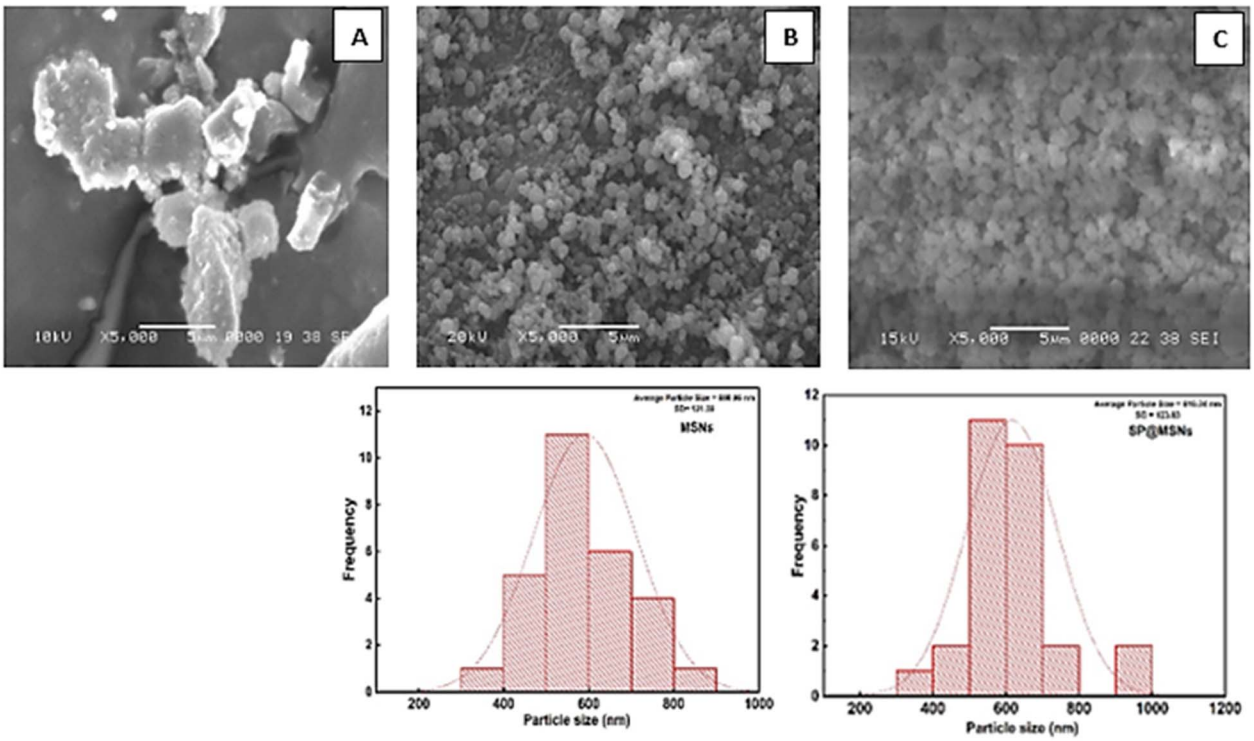

Fig. 4 Scanning electron microscope images of free SP (A), free mesoporous silica (MSNs) (B), and formulated nanoparticles (SP@MSNs) (C); and the particle size histogram calculated by ImageJ for free mesoporous silica (MSNs), and formulated nanoparticles (SP@MSNs).

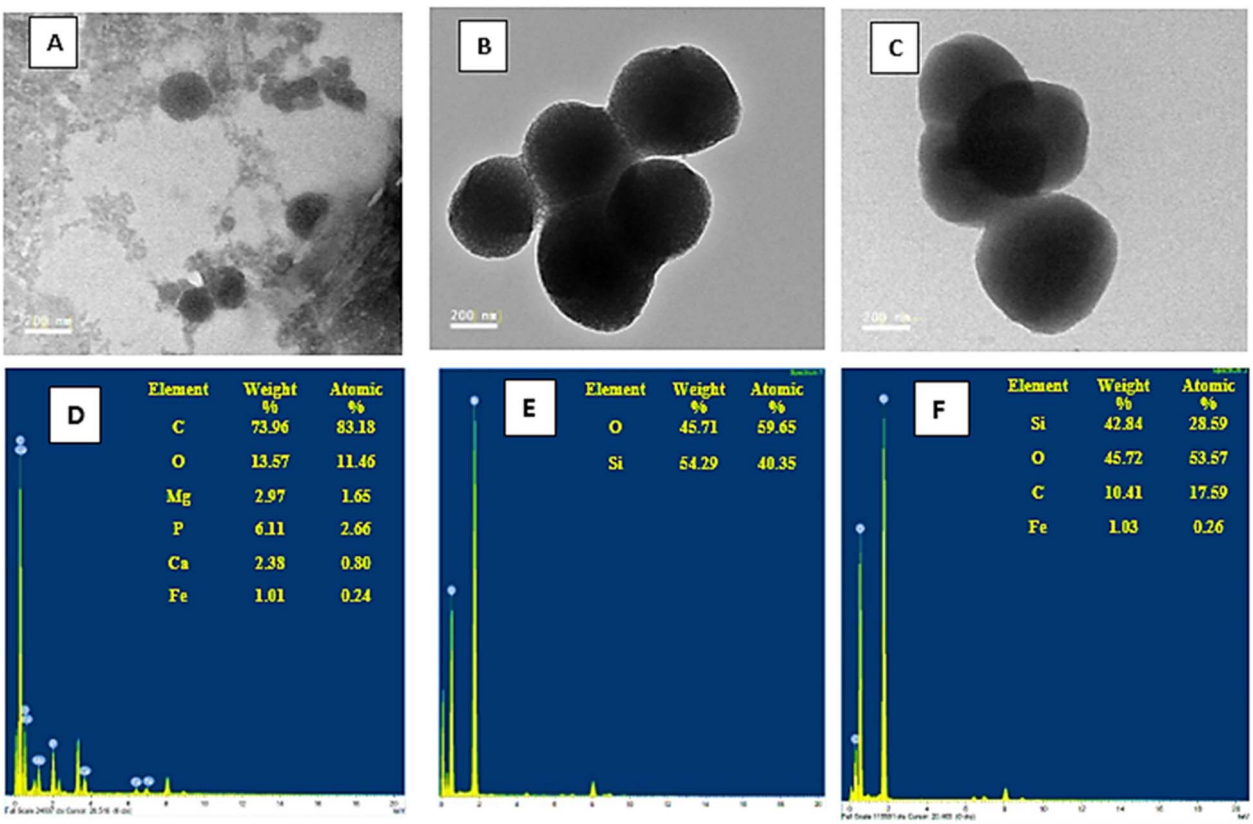

Fig. 5 Transmission electron microscope of free SP (A), free mesoporous silica (MSNs) (B), and formulated nanoparticles (SP@MSNs) (C); and the EDX elemental analysis of free SP (D), free mesoporous silica (MSNs) (E), and formulated nanoparticles (SP@MSNs) (F).

carcinogenesis provides beneficial strategies for basic cancer treatment.

Essentially, direct targeting of the pathways discussed above presents promising therapeutic strategies to modulate the immune system, suppress tumor progression, and overcome the resistance associated with conventional therapies.

3.3. Biosynthesis and characterization of *S. platensis* extract-loaded MSNs (SP@MSNs)

Aligning with our network pharmacology results, the efficacy mechanisms of *S. platensis* bioactive compounds against breast cancer has been clarified through uncovering the main correlated genes and disease pathways from a network aspect. Despite the fact that network pharmacology is a quick and efficient paradigm for predicting multiple therapeutic targets in complex diseases, our network analysis results must be experimentally verified to establish the correlation and effectiveness of *S. platensis* bioactive chemicals against breast cancer. Additionally, in an effort to refine the effectiveness of *S. platensis* bioactives by enhancing their solubility, stability, cellular uptake, targeted delivery, and controlled release, the *S. platensis* extract was encapsulated within the porous structure of mesoporous silica nanoparticles, creating a compatible nanohybrid system. This nanosystem was then optimized and characterized using various techniques, such as microscopy (SEM and TEM), to determine the nano-formulation's size, morphology, and internal structure; spectroscopy (such as FTIR spectroscopy), to examine the chemical interactions; and X-ray diffraction (XRD), to study the crystalline structure. Other important stability parameters, such as surface charge, were monitored through zeta potential measurements as described in the following subsections.

3.3.1. Scanning electron microscopy (SEM). SEM was utilized to characterize the surface morphology, size, and shape of the free SP and the prepared mesoporous silica nanoparticles (MSNs) before and after loading. Fig. 4A, with 40× image magnification, shows an irregular arrangement of the free SP extract particles. Fig. 4B and C show 5000× magnification SEM images of silica nanoparticles before and after drug loading, in which uniformly distributed particles with a spherical appearance and smooth surface are observed. This demonstrates that the technique was successful in synthesizing pure MSNs and that SP particles were loaded inside the mesoporous silica particles.[23]

3.3.2. Transmission electron microscopy (TEM). TEM was used to evaluate the morphological integrity of *S. platensis* ethanolic extract particles (SP) and mesoporous silica nanoparticles (MSNs) before and after loading with SP ethanolic extract. Fig. 5A shows irregular spherical particles of the *S. platensis* ethanolic extract with electron-dense nanoscale structures (80–150 nm) distributed within an amorphous organic matrix. The darker regions correspond to dense biomolecular or pigment-rich domains or could be metal nanoparticles embedded in a biomolecular matrix derived from *Spirulina* compounds; the lighter background indicates low-density organic material. The observed spherical domains are consistent with previous reports describing the nanoscale aggregation of *S. platensis* biomolecules and pigment-derived complexes.[48] Similar TEM observations of amorphous organic matrices and dense nanodomains have been reported for other algal extracts, confirming that phytoconstituents such as proteins and phenolic compounds can self-assemble into stable nanostructures.[49] Fig. 5B shows TEM images of mesoporous silica nanoparticles before drug loading, confirming the presence of mesoporous characteristics across all samples. The lighter grey interior texture suggests the presence of porous channels, typical of mesoporous silica frameworks synthesized using surfactant templates such as CTAB. A spherical appearance, smooth surface with pore structure, and uniformly distributed particle size within the range of 150–200 nm were observed, as indicated by the 200 nm scale bar. The uniformity in particle morphology reflects effective control over the hydrolysis and condensation of tetraethyl orthosilicate (TEOS) during the synthesis, while the absence of structural collapse or irregular shapes confirms the stability of the silica matrix after template removal.[16,24] Therefore, the TEM results confirm that the synthesized MSNs possess the desired nanostructural

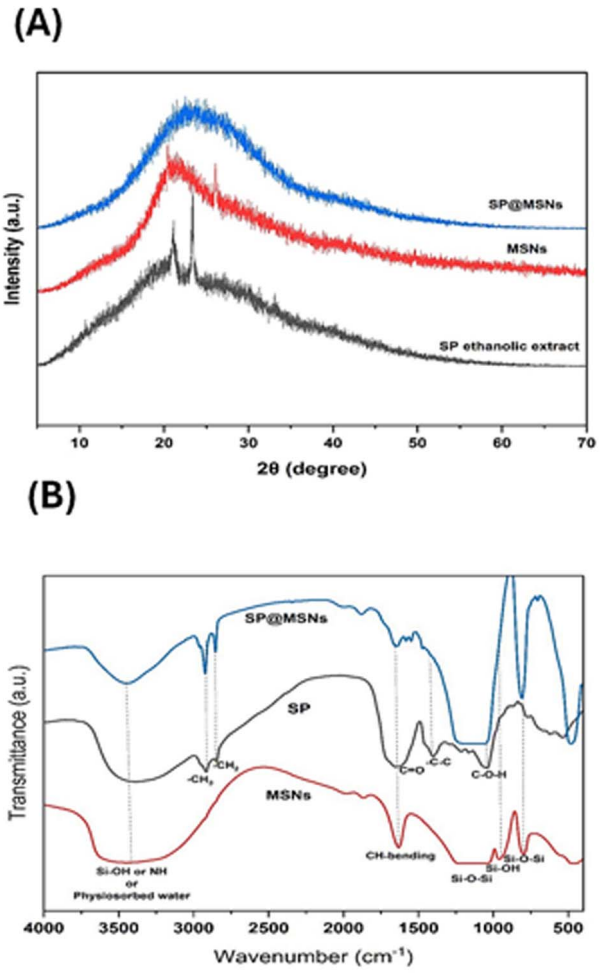

Fig. 6 (A) XRD pattern of SP ethanolic extract, MSNs, and SP@MSNs composite. (B) FTIR spectra of (a) MSNs, (b) free SP ethanolic extract, and (C) SP@MSNs complex.

features suitable for use as efficient carriers for phytoconstituents such as *Spirulina platensis* extract. In Fig. 5C, a TEM image was used to evaluate the morphological integrity of MSNs after loading with *S. platensis* ethanolic extract (SP@MSNs composite). When the silica NPs reacted with SP under the optimal conditions, the size increased, confirming the loading of SP extract into the MSNs. Also, the internal contrast of the particles became notably darker and more homogeneous compared to the pristine MSNs, suggesting successful encapsulation of *Spirulina* phytoconstituents within the mesoporous channels and on the silica surface. The decreased brightness and pore visibility observed in the loaded sample can be attributed to the filling of internal pores and the adsorption of organic molecules, which reduces electron transparency. This observation aligns with earlier reports indicating that the impregnation of silica pores with bioactive compounds or plant extracts often results in the loss of the well-defined porous texture due to the occupation of the mesoporous network by organic moieties.[50] The dense appearance of the nanoparticles also confirmed strong interactions such as hydrogen bonding and electrostatic attractions between the hydroxyl groups on the silica surface and the polar phytochemicals (proteins, polyphenols, and pigments) present in *Spirulina* extract.[16] These morphological changes observed by TEM correlate with complementary characterization data (such as EDX, XRD, FTIR, TGA, and zeta size and potential), confirming that *Spirulina* constituents were effectively loaded within the MSNs without causing aggregation or collapse of the silica framework. The preservation of spherical geometry and the uniform contrast distribution further support the stability of the nanocarrier system, indicating that MSNs can efficiently encapsulate and protect bioactive compounds derived from *S. platensis*.

3.3.3. EDX elemental analysis of SP, MSNs and SP@MSNs. Fig. 5D shows the elemental composition of *S. platensis* ethanolic extract, which was used to evaluate its biochemical richness and suitability as a bioresource. The EDX spectrum of the SP ethanolic extract revealed that carbon (73.96 wt%) and oxygen (13.57 wt%) were the predominant elements, reflecting the high content of organic biomolecules such as proteins, carbohydrates, and lipids. In addition, minor peaks corresponding to magnesium (2.97 wt%), phosphorus (6.11 wt%), calcium (2.38 wt%), and iron (1.01 wt%) were detected, indicating the existence of essential mineral constituents and trace elements. The presence of Mg and Fe supports the photosynthetic origin and metabolic activity of the microalgae. Similar elemental distributions have been reported in previous studies on *S. platensis*, validating its potential as a bioactive and mineral-rich source for green synthesis and biomedical applications.[51,52] As shown in Fig. 5E, the EDX spectrum exhibits strong characteristic peaks corresponding to silicon (Si) (45.71 wt%) and oxygen (54.29 wt%), which are indicative of the silica framework. There were no traces of any other element, confirming the successful removal of the CTAB template. After loading, as shown in Fig. 5F, the EDX spectrum of the SP@MSNs sample exhibits a distinct carbon peak compared to that of the pristine mesoporous silica, confirming the adsorption of organic biomolecules from the *Spirulina* extract onto the silica surface and within its porous network. The presence of additional minor elements, such as iron (Fe), derived from the extract, further supported the successful encapsulation of bioactive compounds within the silica structure; the atomic or weight percentage varied according to the concentration of SP loaded. The Si/O ratio remained close to the stoichiometric value expected for SiO_2, suggesting that the silica framework retained its structural integrity during the loading process. These results indicate the effective impregnation of the SP extract through physical adsorption and hydrogen-bonding interactions between the hydroxyl groups of the silica and the polar functional groups of the biomolecules, in agreement with similar findings reported for microalgae-based extract-loaded mesoporous materials.[16]

3.3.4. X-ray diffraction (XRD). As shown in the diffractograms of the free SP ethanol particles in Fig. 6A, low-intensity peaks are revealed, suggesting that the *Spirulina* extract is amorphous. Small peaks may correspond to organic or biomolecular crystalline components (such as pigments or minor salts), but overall, the structure lacks long-range order. These findings align with earlier findings that confirmed the amorphous nature and size reduction of the free SP ethanolic extract, which could be related to the higher content of hemicellulose in this extract than cellulose.[23] The diffractogram of MSNs, shown in Fig. 6A, exhibits a broad peak centered around $2\theta \approx 22°–25°$ that is characteristic of amorphous silica (SiO_2). This confirms that the MSNs are non-crystalline, which is typical for silica materials synthesized by templated methods.[53] The XRD pattern of the SP@MSNs composite in Fig. 6A remains similar to that of MSNs, with a broad peak around 22°, but the intensity and peak shape change slightly. The slight decrease in intensity or peak broadening indicates successful loading of the *Spirulina* extract into the mesoporous structure. No sharp new peaks appear, suggesting the extract is well dispersed and does not crystallize inside the pores.[16]

3.3.5. Fourier-transform infrared (FTIR) spectroscopy. The FTIR spectra of MSNs, SP, and SP@MSNs were recorded over the wavenumber range from 4000 cm^{-1} to 400 cm^{-1}, as shown in Fig. 6B. The characteristic absorption bands of pure MSNs appeared at 3440 cm^{-1}, 1085 cm^{-1}, 798 cm^{-1}, and 457 cm^{-1}, corresponding to the stretching vibrations of surface silanol groups (Si–OH), Si–O–Si asymmetric stretching, and Si–O bending, respectively, confirming the formation of a silicate framework.[16] The spectrum of free SP ethanolic extract exhibited distinct peaks at 3389 cm^{-1} (O–H or N–H stretching), 2916 and 2847 cm^{-1} (C–H stretching of aliphatic chains), 1652 cm^{-1} (C═O stretching of amide I), and 1215–1039 cm^{-1} (C–O and C–O–C stretching),[54] indicating the presence of proteins, polysaccharides, phenolic compounds, and lipids.[51] The spectrum of SP@MSNs verifies the intermolecular interactions between the SP and the MSNs. The coexistence of silica-related bands (1085 and 798 cm^{-1}) together with the characteristic organic peaks of SP confirms the successful loading of the *Spirulina* ethanolic extract onto the mesoporous silica surface. The slight broadening and shift of the O–H band around 3400 cm^{-1} suggest the formation of hydrogen bonding and physical

adsorption interactions between the hydroxyl groups of the *Spirulina* ethanolic extract (SP) and the silanol groups of MSNs.

3.3.6. Thermogravimetric analysis (TGA). TGA of *S. platensis* ethanolic extract (SP), MSNs, and *Spirulina*-loaded mesoporous silica (SP@MSNs) revealed distinct multi-step weight loss patterns reflecting their compositional and structural characteristics, as shown in Fig. S2. For the *Spirulina* ethanolic extract, an initial weight loss (15.920%) below approximately 200 °C corresponds to the evaporation of physically adsorbed moisture and residual solvent. Three major degradation steps with weight loss (8.940%, 34.268%, and 33.605%) occur between 200 °C and 650 °C, which are attributed to the thermal decomposition of organic constituents such as proteins, carbohydrates, fatty acids, and phenolic compounds, followed by a minor residual weight loss (1.025%) above 650 °C due to the formation of inorganic ash.[23] In contrast, the MSNs exhibit only a slight weight loss of 18.636% (typically below 101 °C) related to the desorption of physically adsorbed water and ethanol, followed by a gradual decrease up to 700 °C, corresponding to the dehydroxylation of surface silanol groups (Si–OH) and the possible removal of trace surfactant residues, confirming their excellent thermal stability and inorganic nature. The SP@MSNs sample shows four distinct thermal stages: the first weight loss stage (1.138%) below 120 °C is attributed to moisture evaporation; the second stage, a pronounced weight loss (3.214%) between 180 °C and 300 °C, is attributed to the loss of physically adsorbed and weakly bound organic molecules at the MSNs surface, The third and major weight loss (5.022%), between 300 °C to 430 °C, is associated with the decomposition of the encapsulated *Spirulina* organic compounds within the silica pores. Finally, a minor weight reduction above 430 °C results from the dehydroxylation of silica and the final breakdown of remaining organic residues. The total weight loss of SP@MSNs is lower than that of the pure extract SP but higher than that of bare MSNs, confirming the successful loading of the extract and the enhanced thermal stability imparted by the silica matrix.

3.3.7. Particle size and zeta potential analyses. As shown in Fig. 7A and Table 2, *Spirulina* extract (SP free particles) exhibited a heterogeneous size distribution with peaks around the submicron and micron ranges. The first peak appears in the submicron range (approximately 190 nm), representing small, dispersed biomolecular particles or nanosized aggregates present in the SP ethanolic extract. The second peak occurs in the micron range (around 800–1000 nm or higher), indicating the presence of larger aggregates or clusters formed by the interaction of biomolecules such as proteins, polysaccharides, and pigments. These findings are consistent with the TEM

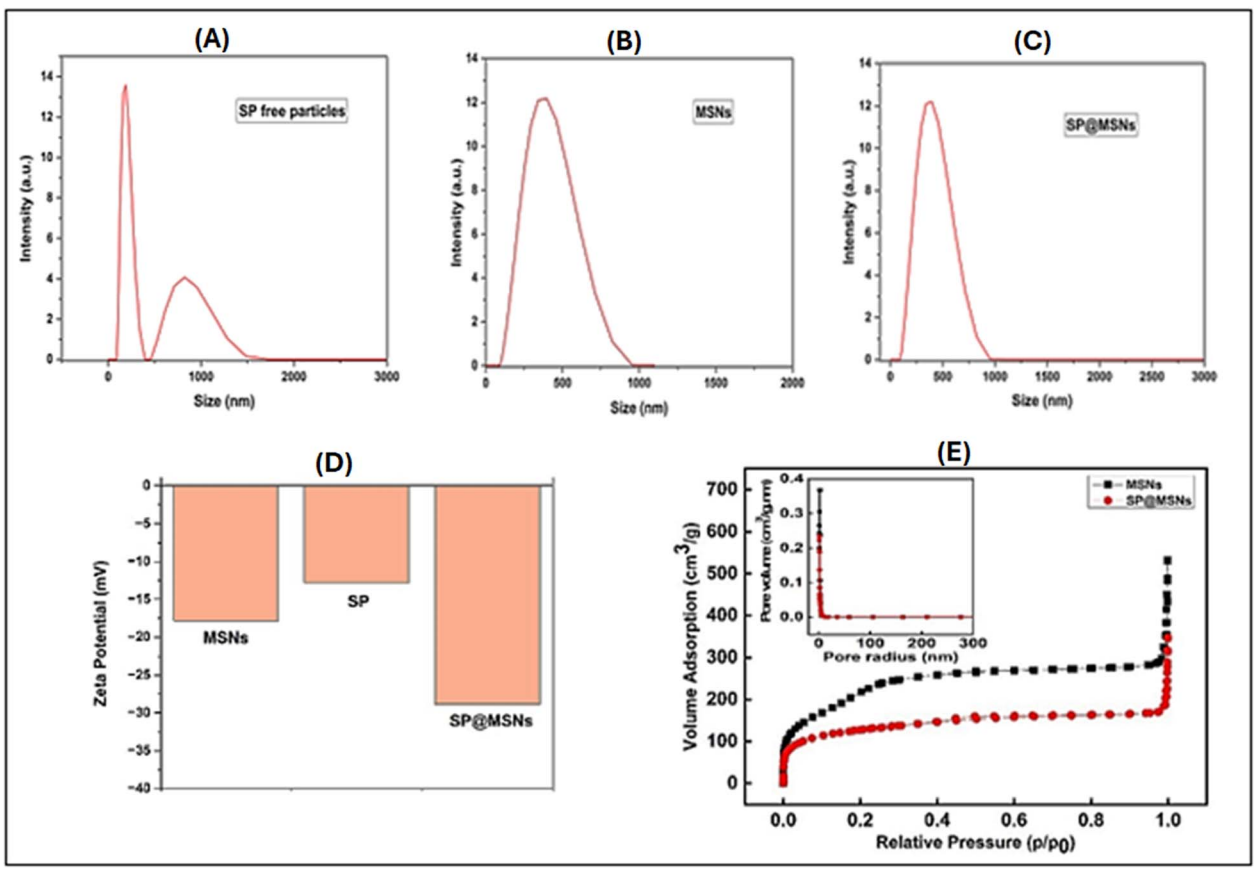

Fig. 7 Particle size and PDI determined by DLS in ethanol for (A) SP, (B) MSNs, (C) SP@MSNs, and (D) their zeta potential (mV). (E) Nitrogen adsorption–desorption isotherms of empty silica nanoparticles (MSNs), and SP-loaded MSNs (SP@MSNs). The insert of (E) shows the BJH pore size distribution of empty mesoporous silica nanoparticles (MSNs), and SP-loaded MSNs (SP@MSNs).

Table 2 Particle size, polydispersity index, and zeta potential of SP, MSNs, SP@MSNs particles dispersed in ethanol and quantitative BET/BJH data for MSNs and SP@MSNs samples[a]

Nano-formulation	Particle size (nm)	PDI	Zeta potential (mV)	$a_{s,\ BET}$ ($m^2\ g^{-1}$)	Average pore diameter (nm)
SP	192.3 ± 53.2853.7 ± 205.1	0.588 ± 0.62	−12.8 ± 13.3		
MSNs	223.6 ± 55.1	0.533 ± 0.76	−17.8 ± 11.8	790.45	2.5085
SP@MSNs	371.6 ± 152.2	0.482 ± 0.92	−28.9 ± 14.4	442.86	2.2843

[a] PDI: polydispersity index, SP: Spirulina, MSNs: mesoporous silica nanoparticles, a_s, BET: Brunauer–Emmett–Teller (BET) surface area.

observations in Fig. 5A. The mesoporous silica nanoparticles (MSNs) showed a single, narrow peak with an average particle size of 223.6 nm (Fig. 7B), confirming their uniform nanoscale size and monodispersity.[53] Upon loading the *Spirulina* extract into the mesoporous silica (SP@MSNs), the average particle size slightly increased compared to bare MSNs (=371.6 nm), suggesting successful encapsulation or adsorption of bioactive molecules from the extract onto the silica surface and within the pores (Fig. 7C). These findings are supported by TEM observations shown in in Fig. 5B and C, which further confirmed the nanoscale size, spherical morphology, and the successful incorporation of SP ethanolic extract within the mesoporous silica framework.

The zeta potential measurements revealed that the mesoporous silica nanoparticles (MSNs) exhibited a negative surface charge of approximately −17 mV, mainly due to surface silanol (Si–OH) groups. *Spirulina* extract (SP) also showed a negative potential of about −13 mV, which can be attributed to negatively charged biomolecules such as fatty acids, polysaccharides, and pigments (Fig. 7D). After loading the SP extract into the silica framework (SP@MSNs), the zeta potential decreased further to around −33 mV, indicating enhanced surface charge due to the adsorption of polar biomolecules and possible electrostatic interactions between the silica surface and the components of the SP extract. This higher negative potential suggests improved colloidal stability and confirms the successful incorporation of *Spirulina* extract within the mesoporous silica matrix.

3.3.8. Pore volume, pore diameter, and specific surface area. The nitrogen adsorption–desorption isotherm measurements, used to evaluate the textural properties of mesoporous silica nanoparticles before and after SP loading, are depicted in Fig. 7E. Pristine MSNs exhibited a typical type IV isotherm with a hysteresis loop,[55] characteristic of mesoporous materials, and showed a high BET specific surface area of 790.45 $m^2\ g^{-1}$ with an average BJH pore diameter of 2.5085 nm (Table 2). After SP loading, the BET surface area decreased markedly to 442.86 $m^2\ g^{-1}$, accompanied by a reduction in average pore diameter to 2.2843 nm, corresponding to decreases of approximately 43.99% and 8.94%, respectively. As shown in Fig. 7E, SP@MSNs displayed significantly reduced nitrogen uptake across the entire relative pressure range compared to bare MSNs. In addition, the BJH pore size distribution revealed a pronounced decrease in pore volume after SP loading. These results confirm the successful incorporation of SP within the mesoporous channels of MSNs through pore filling, while preserving the overall mesoporous framework.

3.3.9. Loading capacity (LC%) and encapsulation efficiency (EE%) evaluation. The loading capacity (LC%) and encapsulation efficiency (EE%) of the SP@MSNs composite were found to be 78.07% and 98.37%, respectively. The exceptionally high EE% indicates that nearly all the extract was successfully incorporated within the mesoporous silica framework, demonstrating the strong affinity between the bioactive compounds and the silica surface. The high LC% further confirms the efficient adsorption and entrapment of *Spirulina* constituents within the nanopores. These results can be attributed to the large surface area, high pore volume, and abundant silanol groups of MSNs, which promote strong hydrogen bonding with the polar biomolecules of the extract. Overall, these findings highlight the excellent loading performance of the mesoporous silica carrier, suggesting its effectiveness in enhancing the stability of *S. platensis* bioactive compounds.

3.4. MTT cytotoxicity assay against (HSF) and (MCF-7) cell lines

3.4.1. Cytotoxicity against normal cells (HSF). First, the cytotoxicity of *S. platensis* extract, mesoporous silica nanoparticles, and the established nano-hybrid formula (SP@MSNs) was screened on Human Foreskin Fibroblasts (HSF) using the MTT assay to ascertain their favorable safety profile and maximize the therapeutic potential by selectively killing cancer cells while sparing healthy ones. As presented in Fig. S3, our results revealed that *S. platensis*, MSNs, and SP@MSNs are generally considered selective and safe with high 50% cytotoxicity concentrations (CC_{50}) against HSF normal cells of 438.6, 244.3, and 514.3 μg mL^{-1}, respectively. Notably, encapsulating *Spirulina* extract within the MSN core–shell increases the safety and biocompatibility of the overall nanocarrier system and the encapsulated extract on the normal cells. Of note, silica itself is generally regarded as safe (GRAS) by the FDA.[56]

3.4.2. Cytotoxicity against breast cancer cells (MCF-7). Secondly, the anti-proliferative potential of *S. platensis* and SP@MSNs was monitored on human breast cancer cell lines (MCF-7) using the MTT assay. The cytotoxicity results toward MCF-7 cells are expressed as half maximal inhibitory concentrations (IC_{50}). As presented in Fig. 8, *S. platensis* extract exerted moderate cytotoxic activities against MCF-7, with a mean IC_{50} value of 119.4 ± 1.4 μg mL^{-1}. Meanwhile, the bioengineered

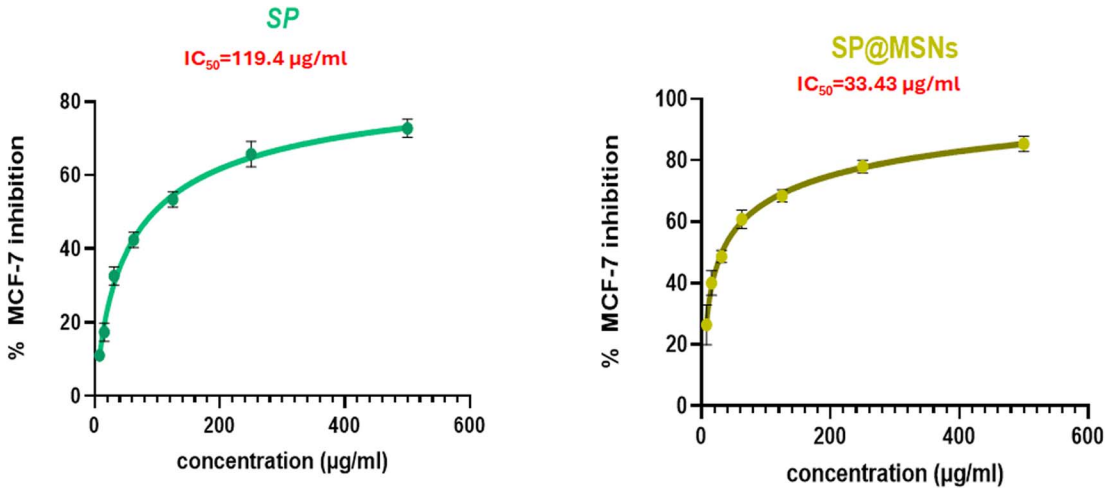

Fig. 8 The dose–response curves revealing the anti-proliferative potential of *S. platensis* and SP@MSNs on human breast cancer cell lines (MCF-7) using the MTT assay, where the results are expressed as half maximal inhibitory concentrations (IC_{50}).

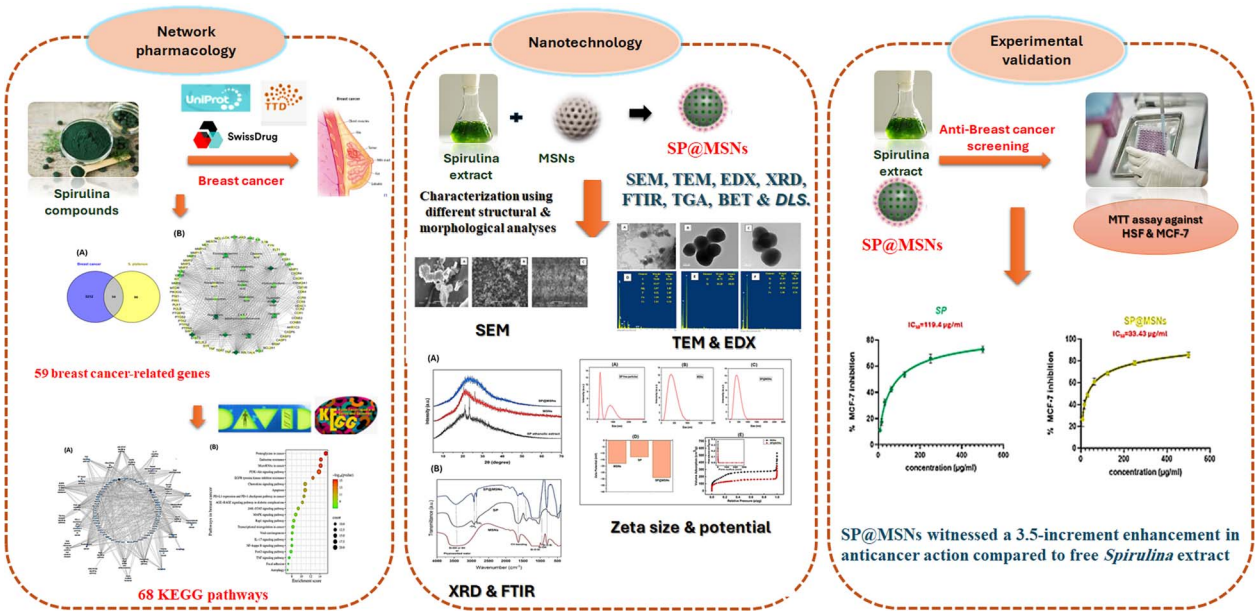

Fig. 9 Simplified diagram outlining the rational workflow of the current study.

nanocomposites of silica and *Spirulina* extracts demonstrated superior anticancer action, with IC_{50} values of 33.6 ± 0.32 µg mL^{-1}. In other words, the anticancer efficacy was enhanced by approximately 3.5-fold in the established nano-hybrid system compared to that of the free *Spirulina* extract.

By encapsulating *Spirulina* compounds within the porous shell of silica nanoparticles, their uptake and effectiveness in biological systems can be greatly enhanced, as the small size and unique properties of nanoparticles allow them to cross biological barriers more easily. Also, the high surface area and porous structure of silica nanoparticles allow a high load of *Spirulina* extract and enable a regulated release of the bioactive compounds instead of an initial "burst" release. Our results are in good harmony with a recent leading investigation that revealed that *Annona muricata* extract conjugated with silica nanoparticles displayed promising cytotoxic potential against the MCF-7 breast cancer cell line, with an IC_{50} value of 33.43 µg mL^{-1} and long-term release of 64% over the course of 12 h, in contrast to the free extract.[57] Equally important, incorporating curcumin into silica nanoparticles exhibited great cytotoxic results against HeLa cell lines due to the enhanced bioavailability and loading capacity of curcumin within the silica nanoparticle matrix.[58]

For ease of tracking, a simplified diagram outlining the rational workflow of the current study is shown in Fig. 9.

4. Conclusion

This study utilized an integrative approach combining network pharmacology, nanotechnology, and experimental validation to evaluate the efficacy of *Spirulina* bioactive compounds against breast cancer. The network pharmacology findings have demonstrated AKT1, SRC, IGFR 1, BCL-2, and EGFR as the top breast cancer genes; these are highly correlated with MicroRNAs in cancer, the PI3K-Akt signaling pathway, EGFR tyrosine kinase inhibitor resistance, and the chemokine signaling pathway, which are modulated by *Spirulina* bioactive compounds, primarily catechin, rosmarinic acid, apigenin, carnosic acid, and eicosapentaenoic acid. Complementarily, a new nanoconjugate based on *Spirulina* extract loaded into the mesoporous silica framework was developed, optimized, and pharmaceutically assessed by different structural and morphological analyses, primarily SEM, TEM, EDX, XRD, and FTIR. Thermal analysis (TGA), along with loading capacity and loading efficiency were also monitored, confirming the effective encapsulation of the extract. Essentially, the SP@MSNs was experimentally screened against normal and breast cancer cells using the MTT assay. Practically speaking, the bioengineered nanocomposites of silica and *Spirulina* extracts have demonstrated promising physicochemical properties and superior anticancer action, with IC_{50} values of 33.43 $\pm$ 0.32 μg mL^{-1}, which is an approximately 3.5-fold enhancement compared with the free *Spirulina* extract, suggesting enhanced loading, stability, bioavailability, and the biological properties of the *Spirulina* compounds. These findings support the potential significance of MSNs as a safe and effective nanocarrier platform for leveraging the therapeutic efficacy of *Spirulina* marine wealth in anticancer applications. Nevertheless, further research, definitive justifications, and adequate clinical proof should be conducted to bolster the biological significance.

Author contributions

Dina S. Ghallab: conceptualization, methodology, data curation, writing–original draft preparation, supervision, validation, writing–reviewing and editing. Doaa A. Ghareeb: methodology, data curation, writing–original draft preparation, supervision. Mazen Sherif: methodology, data curation, writing–original draft preparation, and supervision. Marwa Y. Kenawy: conceptualization, methodology, data curation, writing–original draft preparation, supervision, validation, writing–reviewing and editing.

Conflicts of interest

The authors declare no conflict of interest.

Data availability

Data are provided within the manuscript or supplementary information (SI). Supplementary information is available. See DOI: https://doi.org/10.1039/d5ra08876c.

References

1 A. Leiter, R. R. Veluswamy and J. P. Wisnivesky, *Nat. Rev. Clin. Oncol.*, 2023, **20**, 624–639.
2 L. E. L. Hendriks, J. Remon, C. Faivre-Finn, M. C. Garassino, J. V Heymach, K. M. Kerr, D. S. W. Tan, G. Veronesi and M. Reck, *Nat. Rev. Dis. Prim.*, 2024, **10**, 71.
3 A. Hussain, M.-L. Bourguet-Kondracki, M. Majeed, M. Ibrahim, M. Imran, X.-W. Yang, I. Ahmed, A. A. Altaf, A. A. Khalil and A. Rauf, *Biomed. Pharmacother.*, 2023, **159**, 114165.
4 I. A. Dabban, I. M. Hussaini, M. Ahmed, A. Mohammed and T. Reham, in *Marine Greens*, CRC Press, 2024, pp. 3–14.
5 M. Dimopoulou, A. Kolonas, D. Stagos and O. Gortzi, *Biomass*, 2025, **5**, 11.
6 S. Sahil, S. Bodh and P. Verma, *J. Cell. Biotechnol.*, 2024, **10**, 159–172.
7 G. Prabakaran, P. Sampathkumar, M. Kavisri and M. Moovendhan, *Int. J. Biol. Macromol.*, 2020, **153**, 256–263.
8 N. A. Fadel, M. M. Aziz, G. M. Shafey, R. R. Rashed and H. A. Gheita, *Egypt. Rheumatol.*, 2024, **46**, 38–42.
9 D. S. Ghallab, E. Shawky, A. A. Khalifa, S. S. Elblehi, M. M. Mohyeldin and R. S. Ibrahim, *Naunyn-Schmiedeberg's Arch. Pharmacol.*, 2025, **398**, 15495–15513.
10 M. Akbarizare, H. Ofoghi, M. Hadizadeh and N. Moazami, *Egypt. Liver J.*, 2020, **10**, 1–8.
11 A. Czerwonka, K. Kaławaj, A. Sławińska-Brych, M. K. Lemieszek, M. Bartnik, K. K. Wojtanowski, B. Zdzisińska and W. Rzeski, *Biomed. Pharmacother.*, 2018, **106**, 292–302.
12 A. Shah, V. Patel, M. Jain and G. Parmar, in *CADD and Informatics in Drug Discovery*, Springer, 2023, pp. 231–252.
13 M. Ahmad, M. Tahir, Z. Hong, M. A. Zia, H. Rafeeq, M. S. Ahmad, S. ur Rehman and J. Sun, *Front. Pharmacol*, 2025, **15**, 1497668.
14 N. Bhusare, A. Gade and M. S. Kumar, *J. Biochem. Mol. Toxicol.*, 2024, **38**, e23732.
15 S. Vrignaud, J.-P. Benoit and P. Saulnier, *Biomaterials*, 2011, **32**, 8593–8604.
16 D. L. Aulifa, B. Amarilis, L. N. Ichsani, D. S. Maharani, A. M. Shabrina, H. Hanifah, R. P. Wulandari, A. Rusdin, L. Subra and A. Budiman, *Pharmaceuticals*, 2024, **17**, 1684.
17 F. Aghapour, A. A. Moghadamnia, A. Nicolini, S. N. M. Kani, L. Barari, P. Morakabati, L. Rezazadeh and S. Kazemi, *Biochem. Biophys. Res. Commun.*, 2018, **500**, 860–865.
18 H. A. Hussein, M. S. Nazir, N. Azra, Z. Qamar, A. Seeni, T. A. D. A.-A. Tengku Din and M. A. Abdullah, *Mar. Drugs*, 2022, **20**, 480.
19 M.-H. Tsou, Z.-Y. Wu, G. Chen, C.-C. Lee, Z.-H. Lee, W. T. Yuan, S.-M. Lin and H.-M. Lin, *Int. J. Biol. Macromol.*, 2023, **253**, 127078.
20 D. S. Ghallab, E. Shawky, R. S. Ibrahim and M. M. Mohyeldin, *Sci. Rep.*, 2022, **12**, 8094.
21 E. Zanganeh, H. Mirzaei, S. M. Jafari, A. Javadi and M. R. Afshar Mogaddam, *J. AOAC Int.*, 2022, **105**, 827–834.

22 S. M. Khedr, D. A. Ghareeb, S. A. Fathy and G. M. Hamdy, *BMC Pharmacol. Toxicol.*, 2023, **24**, 42.
23 M. Almukainzi, T. A. El-Masry, H. A. Ibrahim, H. M. Saad, E. I. El Zahaby, A. Saleh and M. M. F. El-Nagar, *Mar. Drugs*, 2024, **22**, 395.
24 M. L. Ruiz-González, A. Torres-Pardo and J. M. González-Calbet, *Pharmaceutics*, 2021, **13**, 2200.
25 K. Rathod, H. Ahmed, S. S. Gomte, S. Chougule, M. R. Dethe, R. J. Patel, D. B. PVP and A. Alexander, *J. Solid State Chem.*, 2023, **317**, 123639.
26 D. Campoccia, S. Ravaioli, S. Santi, V. Mariani, C. Santarcangelo, A. De Filippis, L. Montanaro, C. R. Arciola and M. Daglia, *Biomed. Pharmacother.*, 2021, **141**, 111895.
27 P. Kumar, A. Nagarajan and P. D. Uchil, *Cold spring Harb. Protoc.*, 2018, **2018**, pdb–prot095505.
28 R. Zhang, X. Zhu, H. Bai and K. Ning, *Front. Pharmacol*, 2019, **10**, 123.
29 D. S. Ghallab, Z. M. Awwad, R. S. Ibrahim and E. Shawky, *Food Biosci.*, 2025, **69**, 106863.
30 R. E. Mutha, A. U. Tatiya and S. J. Surana, *Futur. J. Pharm. Sci.*, 2021, **7**, 25.
31 P. Pandey, F. Khan, S. A. Seifeldin, K. Alshaghdali, S. Siddiqui, M. E. Abdelwadoud, M. Vyas, M. Saeed, A. Mazumder and A. Saeed, *Nutrients*, 2023, **15**, 2088.
32 X. Liao, Y. Gao, L. Sun, J. Liu, H. Chen, L. Yu, Z. Chen, W. Chen and L. Lin, *Phyther. Res.*, 2020, **34**, 1142–1153.
33 M. J. González-Fernández, I. Ortea and J. L. Guil-Guerrero, *Toxicol. Res. (Camb).*, 2020, **9**, 474–483.
34 L. Zhao, J. Zhang, Y. Fan and Y. Li, *Med. Sci. Monit. Int. Med. J. Exp. Clin. Res.*, 2019, **25**, 7864.
35 A. Nicolini, P. Ferrari, L. Kotlarova, G. Rossi and P. M. Biava, *Curr. Pharm. Biotechnol.*, 2015, **16**, 804–815.
36 S. T. Liu, H. Pham, S. J. Pandol and A. Ptasznik, *Front. Physiol.*, 2014, **4**, 416.
37 H. Cao, G. Wang, L. Meng, H. Shen, Z. Feng, Q. Liu and J. Du, *PLoS One*, 2012, **7**, e49884.
38 S. Halder, S. Basu, S. P. Lall, A. K. Ganti, S. K. Batra and P. Seshacharyulu, *Expert Opin. Ther. Targets*, 2023, **27**, 305–324.
39 S. Khan, L. Cao, J. Wiegand, P. Zhang, M. Zajac-Kaye, F. J. Kaye, G. Zheng and D. Zhou, *Cells*, 2024, **13**, 528.
40 M. Qiang, Z. Chen, H. Liu, J. Dong, K. Gong, X. Zhang, P. Huo, J. Zhu, Y. Shao and J. Ma, *Front. Pharmacol*, 2025, **16**, 1516583.
41 A. Di Lorenzo, E. Bolli, L. Tarone, F. Cavallo and L. Conti, *Int. J. Mol. Sci.*, 2020, **21**, 9418.
42 S. Rawat, K. Dhaundhiyal, I. S. Dhramshaktu, M. S. Hussain and G. Gupta, in *Immunotherapy against Lung Cancer: Emerging Opportunities and Challenges*, Springer, 2024, pp. 247–264.
43 O. V Serzhantova, A. G. Novikova, A. A. Mikhailov, I. P. Moshurov and A. P. Gureev, *Russ. J. Genet.*, 2024, **60**, 647–664.
44 M. P. Rangel, V. K. de Sá, T. Prieto, J. R. M. Martins, E. R. Olivieri, D. Carraro, T. Takagaki and V. L. Capelozzi, *Glycoconj. J.*, 2018, **35**, 233–242.
45 D. Miricescu, A. Totan, I.-I. Stanescu-Spinu, S. C. Badoiu, C. Stefani and M. Greabu, *Int. J. Mol. Sci.*, 2020, **22**, 173.
46 Y. Zhao, Y. He, W. Wang, Q. Cai, F. Ge, Z. Chen, J. Zheng, Y. Zhang, H. Deng and Y. Chen, *Lancet Oncol.*, 2024, **25**, 1347–1356.
47 H. Jung and S. Paust, *Front. Immunol.*, 2024, **15**, 1443366.
48 A. Ivanova, M. Todorova, D. Petrov, Z. Petkova, O. Teneva, G. Antova, M. Angelova-Romova, V. Yanakieva, S. Tsoneva and V. Gledacheva, *Nanomaterials*, 2025, **15**, 1392.
49 W. Xiaokang, J. G. Lyng, N. P. Brunton, L. Cody, J.-C. Jacquier, S. M. Harrison and K. Papoutsis, *Biotechnol. Rep.*, 2020, **27**, e00504.
50 S. Man, W. Liu, J. Bi, J. Bai, Q. Wu, B. Hu, J. Hu and L. Ma, *J. Agric. Food Chem.*, 2024, **72**, 25743–25754.
51 M. P. Spínola, A. R. Mendes and J. A. M. Prates, *Foods*, 2024, **13**, 3656.
52 A. Rahim, C. Çakir, M. Ozturk, B. Şahin, A. Soulaimani, M. Sibaoueih, B. Nasser, R. Eddoha, A. Essamadi and B. El Amiri, *South African J. Bot.*, 2021, **141**, 235–242.
53 N. I. Vazquez, Z. Gonzalez, B. Ferrari and Y. Castro, *Boletín la Soc. Española Cerámica y Vidr.*, 2017, **56**, 139–145.
54 E. Gunasundari, P. Senthil Kumar, F. C. Christopher, T. Arumugam and A. Saravanan, *IET Nanobiotechnol.*, 2017, **11**, 754–758.
55 M. Ulfa, D. Prasetyoko, W. Trisunaryanti, H. Bahruji, Z. A. Fadila and N. A. Sholeha, *Sci. Rep.*, 2022, **12**, 15271.
56 T. I. Janjua, Y. Cao, F. Kleitz, M. Linden, C. Yu and A. Popat, *Adv. Drug Deliv. Rev.*, 2023, **203**, 115115.
57 G. K. Perinbarajan, B. J. Sinclair, A.-T. Mossa, N. Ohja and P. G. Jeelani, *Heliyon*, 2024, **10**, e25048.
58 R. K. Gangwar, G. B. Tomar, V. A. Dhumale, S. Zinjarde, R. B. Sharma and S. Datar, *J. Agric. Food Chem.*, 2013, **61**, 9632–9637.